Applied Geochemistry 100 (2019) 190–202

Contents lists available at ScienceDirect

Applied Geochemistry

journal homepage: www.elsevier.com/locate/apgeochem

Cation exchange and surface complexation of lead on montmorillonite and illite including competitive adsorption effects

M. Marques Fernandes*[,1], B. Baeyens

Paul Scherrer Institute, Laboratory for Waste Management, 5232, Villigen PSI, Switzerland

ARTICLE INFO

Editorial handling by Dr J Lützenkirchen

Keywords:
Dioctahedral clay minerals
Divalent lead
Surface complexation
Cation exchange
Competitive adsorption
Thermodynamic adsorption modelling

ABSTRACT

The adsorption of divalent lead on the homoionic Na forms of illite (Na-IdP) and montmorillonite (Na-SWy) was investigated by batch type adsorption experiments. Ion equilibrium experiments between Pb^{2+} and Na^{+} yielded selectivity coefficients for cation exchange on the planar sites of both clay minerals. Pb adsorption edges (pH 2–11) and isotherms (pH 3, 6 and 7 and at 10^{-12} M < $[Pb_{eql}]$ < 10^{-3} M) were measured and modelled with the two site protolysis non electrostatic surface complexation and cation exchange (2SPNE SC/CE) model. The surface complexation constants derived from an iterative fitting of the edges and isotherms could describe all of the Pb adsorption data sets satisfactorily. The anomalous adsorption behaviour of trace Pb on Na-IdP in the acidic region required the consideration of an additional site with a low capacity and high affinity and an associated pH independent surface complexation reaction. Adsorption experiments with Pb/Ni, Pb/Co, Pb/Zn and Pb/Eu on Na-IdP indicated, depending on the experimental set-up, partially and/or non-competitive behaviour. The competitive adsorption experiments could be quantitatively described with a modified 2SPNE SC/CE model. In the case of non-competitive adsorption additional metal specific sets of strong sites are required. In the case of partial competitiveness, a certain fraction of the strong site capacity is assumed to be competitive whereas the remaining fraction is non-competitive.

1. Introduction

Retention on mineral phases is a key process for the immobilization of metal contaminants in natural or engineered environments and is intrinsically related to the nature of mineral surfaces and the prevailing geochemical conditions. Diocthahedral alumina-silicates such as montmorillonite and illite are important mineralogical components of soils and sedimentary rocks which limit the rate of movement of (radio-) contaminants in natural systems through their exceptional bulk physical and chemical properties (Bergaya and Lagaly, 2013; Borisover and Davis, 2015). Clay minerals control to a large extent most important characteristics of many soils and sediments (e.g., structure, permeability, swelling, cation exchange, pH buffering, retention of micronutrients or (radio-)contaminants) (Dixon, 1991). Owing these unique properties, clay based systems are commonly used for the remediation of contaminated soils and waters (Wagner, 2013; Xu et al., 2017; Yuan et al., 2013; Zhu et al., 2016) and are considered as geological (host rock) and engineered barriers (bentonite) in many deep geological radioactive waste repository concepts (Altmann, 2008; Andra, 2001; Nagra, 2002; Ondraf, 2001).

Thermodynamic adsorption models are key tools for predicting the retention and speciation of contaminants in environments (natural or engineered) and for improving the reliability of assumptions made in risk assessment scenarios (Groenenberg and Lofts, 2014; OECD/NEA, 2012; Payne et al., 2013). Therefore it is highly important to develop a fundamental understanding of the uptake processes onto clay minerals and to implement adsorption models to account for all relevant geochemical parameters to reliably predict their fate in natural environments as well as in the near- and far-fields of radioactive waste repositories.

Lead (Pb) together with arsenic, cadmium and mercury are internationally classified as extremely toxic heavy metal, and considered amongst the elements of major health concern (ATSDR, 2007; IPCS, 1977, 1989a, b, 1991, 1992a, b, 1995, 2001). Pb is released in the environment essentially by anthropogenic activities such as e.g., fossil fuels burning, mining, smelting, recycling and lead-acid batteries. Pb, however, is also of concern in the safety assessment of radioactive waste repositories since it is contained in substantial quantities in radioactive waste originating from e.g., spallation targets, shielding (Nagra, 2014).

* Corresponding author.
E-mail address: maria.marques@psi.ch (M.M. Fernandes).
[1] Present address: Laboratory for Waste Management, Paul Scherrer Institute, 5232 Villigen PSI, Switzerland.

https://doi.org/10.1016/j.apgeochem.2018.11.005
Received 29 March 2018; Received in revised form 31 October 2018; Accepted 8 November 2018
Available online 14 November 2018
0883-2927/ © 2018 Elsevier Ltd. All rights reserved.

A large number of studies can be found in the open literature studying the adsorption of lead on clays macroscopically, however, not many addressed the issue in terms of adsorption quantification and subsequent development of thermodynamic adsorption models (e.g., Akafia et al., 2011; Barbier et al., 2000; Bittel and Miller, 1974; Breen et al., 1999; Coles and Yong, 2002; Farrah and F. Pickering, 1977; Gu et al., 2010; Hefne et al., 2008; Hizal and Apak, 2006; Li et al., 2017; Majone et al., 1993; Majone et al., 1996; Mhamdi et al., 2013; Oubagaranadin and Murthy, 2009; Ozdes et al., 2011; Sari et al., 2007; Scrudato and Estes, 1975; Strawn and Sparks, 1999; Uddin, 2017; Ulrich and Degueldre, 1993; Xu et al., 2008; Yang et al., 2010; Zhang and Hou, 2008). X-ray absorption spectroscopy (XAS) studies investigating the adsorption mechanisms of Pb on clay mineral surfaces at the molecular scale are very sparse (e.g., (Gräfe et al., 2007; Strawn and Sparks, 1999). This scarcity is partly explained by the complex coordination chemistry of Pb and the intrinsic difficulties associated with Pb XAS (i.e., strong deformation of the coordination polyhedral (lone pair electrons), high variability of the coordination numbers and distances, static and dynamic structural disorder, high thermal motion (Manceau et al., 1996)) which affect the sensitivity of XAS to the local structure of lead and complicate spectral analysis.

The two site protolysis non electrostatic surface complexation and cation exchange (2SPNE SC/CE) model has been developed based on large sets of experimental data on purified montmorillonite and illite and has been successfully applied to quantitatively describe the uptake of numerous sorbates with oxidation state ranging from +I to + VI (Bradbury and Baeyens, 1997, 2005b, 2009a, b). As a continuation of the above work, the present study aims in a first part at determining experimentally the adsorption of Pb on montmorillonite and illite to derive thermodynamic constants for the cation exchange (CE) and surface complexation (SC) reactions controlling the adsorption of Pb.

In a second part of this study, the impact of high element concentrations on the adsorption of metals on clay minerals in terms of competitive adsorption is investigated. In soils and sediments, the pool of stable elements is large; metals can be found in the soil/sediment interstitial water, adsorbed on solid phases (often on clay minerals), and as part of the bulk structure of solid phases (e.g., pure phases (solubility limiting), neo-formed solids, solid-solutions). In a deep geological radioactive waste repository sources for stable nuclides are also manifold i.e., porewaters, tunnel back fill materials, host rock formation, corrosion of the carbon steel canister, or by dissolution of spent fuel and vitrified high-level waste. Hence, the influence of the intrinsic metal inventory needs to be quantified since stable elements and released radionuclides may compete with one another for the adsorption sites on the backfill material and the host rock, and thus reduce their uptake on them. Competition of metals adsorbing by SC on clay minerals has so far been little systematically studied (e.g., Atanassova, 1999; Donat et al., 2005; Helios-Rybicka and Wójcik, 2012; Sheikhhosseini et al., 2013; Soltermann et al., 2014b; Yang et al., 2015; Zhu et al., 2011). Bradbury and Baeyens (2005a) investigated the competitive adsorption between different metals (i.e., Cd^{II}, Ni^{II}, Zn^{II}, Eu^{III}, Nd^{III}, Am^{III}, Th^{IV} and U^{VI}) on montmorillonite and concluded that metals with similar chemical properties (e.g., valence state, hydrolysis behaviour) do compete, whereas metals with dissimilar chemistries do not compete. In its present form, the 2SPNE SC/CE model intrinsically considers that metals compete with each other for the adsorption sites since only one common set of strong and weak edge sites are considered for all elements, irrespective of their valence. De facto, the influence of competitive adsorption is not specifically accounted for in the model, except for CE reactions, where cations compete with one another for the planar sites according to the value of their respective selectivity coefficients. Particularly, adsorption on the strong sites could be affected by competitive effects. To ensure the future applicability of the 2SPNE SC/CE model it is important to implement the model, so that adsorption in complex systems closer to reality can be reliably predicted. To this end, it is necessary to identify and quantify the competitive behaviour of safety relevant elements. In the present study, the competitive adsorption between Pb/Ni, Pb/Zn, Pb/Co and Pb/Eu on illite was investigated.

2. Materials and methods

2.1. Clay minerals

SWy-2 montmorillonite (Crook County, Wyoming) was obtained in a powdered form from the Source Clay Minerals Repository, University of Missouri, Columbia. The source illite (Illite du Puy) material was collected from an Oligocene geological formation in the region of Le Puy-en-Velay (Haute-Loire), France (Gabis, 1958). Samples of illite were crushed, and then powdered in a mortar to obtain a particle size $\leq 63\,\mu m$. Both clays were several times washed with 1 M NaCl to remove soluble salts and/or sparingly soluble minerals such as calcite and to convert the clay into the homoionic Na-form. The clay fraction $< 0.5\,\mu m$ was obtained after following steps: successive washing (peptisation) with deionised water pre-equilibrated with the respective clay, centrifugation (~ 7 min at ~ 600 g (max.)), subsequent collection of the supernatant suspension, and finally flocculation with 1 M NaCl. Soluble hydroxy-aluminum compounds and other acid soluble impurities were removed by washing the clay suspension with a 0.1 M NaCl solution at pH 3.5 during 1h (Baeyens and Bradbury, 1997). In the case of IdP a repeated acid washing was carried out (Bradbury and Baeyens, 2009a). Conversion to the 0.1 M NaCl background concentration was achieved by using the dialysis technique. Finally, the conditioned Na-clay suspensions were diluted to a sorbent concentration (S) of $\sim 20\,g{\cdot}L^{-1}$ with the equilibrium solution and stored in the dark at 4 °C. The exact clay content of each batch was determined by drying to constant weight at 105 °C and correcting for the salt content. The end products were suspensions of the respective purified clays in the Na-form which were used as sources for the adsorption experiments.

The cation exchange capacity (CEC) of the purified IdP and SWy was measured by the ^{134}Cs isotopic dilution method (Baeyens and Bradbury, 2004). A large number of CEC determinations on different clay batches carried out at neutral pH, yielded average values of 225 ± 10 $meq{\cdot}kg^{-1}$ and 870 ± 35 $meq{\cdot}kg^{-1}$ for IdP and SWy, respectively.

2.2. Adsorption experiments

Four types of batch adsorption measurements were carried out on Na-SWy and/or Na-IdP: (i) Pb^{2+}-Na^{+} cation exchange (CE) experiments; (ii) Pb adsorption edges (pH dependent adsorption of trace Pb at fixed ionic strength); (iii) Pb adsorption isotherms (concentration dependent Pb adsorption at fixed pH and background electrolyte concentration) and (iv) competitive adsorption experiments between Pb and Zn, Ni, Co and Eu at fixed pH and fixed background electrolyte concentration. The latter were only performed on Na-IdP.

The adsorption edges and isotherms at pH 6 and 7 were measured in controlled N_2 atmosphere glove boxes ($CO_2 \leq 1$ ppm, $O_2 \leq 1$ ppm), whereas the CE and competitive adsorption measurements (including the reference Pb isotherm on Na-IdP at pH ~7) were carried under atmospheric air conditions. Samples were prepared in 40 ml polypropylene centrifuge tubes in duplicates or triplicates. Supra-pure grade chemicals and ultrapure deionised water were used to prepare all the solutions. The adsorption of Pb, Zn, Ni, Co and Eu was quantified by radiochemical assay using the corresponding radioisotopes. ^{57}Co ($t_{1/2}$ = 271.8 d), ^{63}Ni ($t_{1/2}$ = 100 y) and ^{152}Eu ($t_{1/2}$ = 13.3 y) were

Table 1
Summary of the Pb adsorption experiments on Na-IdP and Na-SWy.

Clay	Experiment	$[Pb]_{init/eql}$ (M)[a]	Background electrolyte	S (g L^{-1})	pH
Na-IdP	CE	$2.5{\cdot}10^{-4}$–$2.5{\cdot}10^{-3}$	0.011 N[b]	13.5	4.6–5.6
	Edge	$4{\cdot}10^{-10}$	0.1 M NaCl	1.8	1.5–9.5
	Isotherm	10^{-10}–$2.7{\cdot}10^{-3}$	0.1 M NaCl	1.5–1.9	3.1–3.2
	Isotherm	10^{-10}–$2.7{\cdot}10^{-3}$	0.3 M NaCl	1.7	3.0–3.1
	Isotherm	10^{-12} – $3{\cdot}10^{-4}$	0.02 M NaCl	2.6	5.9–6.1
	Isotherm	10^{-12}–10^{-4}	0.1 M NaCl	1.8–2.6	6.7–7.2
	Isotherm[c]	$4{\cdot}10^{-9}$–10^{-4}	0.1 M NaCl	2.0	6.7–7.2
Na-SWy	CE	$2.5{\cdot}10^{-4}$–$2.5{\cdot}10^{-3}$	0.011 N[b]	4.4	5.0–5.4
	Edge	$4{\cdot}10^{-10}$ and 10^{-6}	0.1 M NaCl	1.1–1.6	2.1–9.9
	Isotherm	$2{\cdot}10^{-10}$–$8{\cdot}10^{-4}$	0.1 M NaCl	1.8	5.9–6.0
	Isotherm	$3{\cdot}10^{-12}$–$5{\cdot}10^{-4}$	0.1 M NaCl	1.7–2.6	6.9–7.0

[a] For the isotherms, Pb equilibrium concentrations are given; for CE and edge measurements, the initial Pb concentrations.
[b] Total normality: total (Pb^{2+} + Na^{+}) concentration in eq·L^{-1}.
[c] Pb reference isotherm for competition experiments carried out under atmospheric air conditions.

purchased from Eckert and Ziegler, Isotope Products Laboratories (California, USA) and ^{65}Zn ($t_{1/2}$ = 343.9 d) from Perkin Elmer, Inc. (Waltham, MA, USA). ^{210}Pb ($t_{1/2}$ = 22.3 y) was obtained from the former Laboratoire de Mesure des Rayonnements Ionisants (LMRI), (CEA, France). For ^{57}Co/^{63}Ni/^{152}Eu and ^{210}Pb, the isotopic composition and stable carrier concentration was provided by the manufacturer or determined in-house by ICP-MS, respectively. The radiotracers contained no other metal impurities. Each source radioisotope solution was diluted in deionised water to produce an acidic stock solution. Standard solutions for use in the adsorption experiments were prepared by labelling aliquots of the given radiotracer stock solution in the background electrolyte (Table 1). Each standard solution was allowed to stand at least overnight before use to ensure equilibrium (wall sorption).

Different buffers i.e., $CH_3COONa{\cdot}3H_2O$ (sodium acetate), $C_6H_{13}NO_4S$ (MES), $C_7H_{15}NO_4S$ (MOPS), $H_2NC(CH_2OH)_3$ (TRIS) or $C_8H_{17}NO_3S$ (CHES) (BioChemika MicroSelect, Fluka) were used at concentrations of $2{\cdot}10^{-3}$ M to prevent pH drift in the adsorption experiments.

For the isotherms, stable Pb, Ni and Eu solutions covering various concentration ranges were prepared at given pH in NaCl background electrolyte (see Table 1). Following salts were used: $Pb(NO_3)_2$ (Puratronic 99.999%, Alfa Aesar), $Ni(NO_3)_2{\cdot}6H_2O$ (for analysis EMSURE, Merck) and $Eu(NO_3)_3{\cdot}5H_2O$ (99.9% trace metals basis, Sigma Aldrich). For each element, the highest metal concentration used was based on thermodynamic solubility calculations. The concentrations and stability of the solutions were verified by ICP-OES measurement.

Generally, the batch type experimental approach consisted of equilibrating over a defined period of time, by end-over-end shaking, aliquots of Na-IdP or Na-SWy suspensions with the radioisotope labelled standard solutions (pH edge) or stable metal solutions (isotherms, CE and competition experiments). Phase separation was obtained using a Beckman Coulter Avanti™ J30i High-Performance centrifuge (1 h at 108,000*g* max.) and aliquots of the supernatants were radiometrically assayed. The pH of the supernatant of each sample was measured using a Metrohm combined electrode. The electrode was calibrated against commercially Merck™ buffers for pH 4, 7 and 10. Radioassay of aliquots of the supernatants as well as of the labelled standard solutions (prepared simultaneously at the start of the adsorption experiments) were carried using a Canberra Packard Tri-Carb 2250 CA liquid scintillation counter (LSC) for ^{63}Ni and ^{210}Pb and a Canberra Packard Cobra Quantum gamma counter for ^{65}Zn and ^{152}Eu. In the Pb stock solution, ^{210}Bi and ^{210}Po were in secular equilibrium with ^{210}Pb. The contribution of ^{210}Bi and ^{210}Po in the LSC spectra were separated by setting different energy windows, as described in Ulrich and Degueldre (1993) and by performing the LSC measurement 30 days after sampling.

Pb^{2+}-Na^{+} CE experiments were carried out on both clay minerals prior converted to 0.01 M NaCl background electrolyte by using the dialysis technique. Aliquots of the respective clay mineral suspension were equilibrated for three days with ^{210}Pb labelled solutions containing stable Pb and Na in different proportions. The total normality of the clay-Na-Pb suspension was kept constant at 0.011 N and the Pb fractional occupancies (N_{Pb}) ranged from 0.1 to 0.9.

Pb adsorption edges were obtained by equilibrating trace ^{210}Pb concentrations with Na-IdP or Na-SWy in the pH range ~2–10 in 0.1 M NaCl. Pb adsorption isotherms were measured by contacting a series of stable Pb solutions covering the required Pb concentration range and labelled with trace ^{210}Pb with both clays at fixed pH and constant ionic strength. Equilibration times for isotherms and edges were 7 days. Further experimental details (i.e., S, pH, concentration range) are summarized in Table 1.

Competitive adsorption on Na-IdP was investigated by determining the adsorption of one element at very low concentration (trace element) in the presence of a competing element (blocking element), whose concentration varied from trace to relatively high concentrations. The aim of these experiments was to progressively increase the blocking metal concentration and simultaneously track the adsorption of the trace metal to see whether it still accesses the strong sites or only adsorbs on the weak and CE sites once the blocking element has fully saturated the strong sites. To quantify and model the competitive influence of the single elements, the adsorption isotherm of the blocking element (reference isotherm) and the adsorption values of the trace element along the blocking element isotherm are necessary. The latter were experimentally obtained in a similar way as the isotherms except that the stable blocking metal solutions were labelled with the radiotracer of the selected trace element. Only binary combinations were considered.

The adsorption of trace Ni, Co, Zn and Eu was measured as function of increasing Pb concentrations on Na-IdP. In a reciprocal set of experiments, the influence of increasing Ni and Eu concentration on the adsorption of trace Pb was quantified. Reference isotherms for Pb, Ni and Eu were measured in the absence of trace metal. The pH varied between 6.7 (at the highest blocking element concentration) and 7.2 (at

Table 2
Summary of competitive adsorption experiments on Na-IdP in 0.1 M NaCl at pH 7 ± 0.3.

Trace metal		Blocking metal		S (g L^{-1})
Me	$[Me]_{init}$ (M)	Me	$[Me]_{eql}$ (M)	
Ni	$3.5{\cdot}10^{-8}$	Pb	$4{\cdot}10^{-9}$–10^{-4}	2.0
Co	$6.0{\cdot}10^{-11}$	Pb	$4{\cdot}10^{-9}$–10^{-4}	2.0
Zn	$1.2{\cdot}10^{-7}$	Pb	$4{\cdot}10^{-9}$–10^{-4}	2.0
Eu	$4.6{\cdot}10^{-9}$	Pb	$4{\cdot}10^{-9}$–10^{-4}	2.0
Pb	$5.9{\cdot}10^{-10}$	Ni	$5{\cdot}10^{-9}$–$6{\cdot}10^{-5}$	1.3
Pb	$8.7{\cdot}10^{-9}$	Eu	$4{\cdot}10^{-10}$–10^{-3}	2.0
–	–	Ni[a]	$4{\cdot}10^{-10}$–10^{-3}	1.3
–	–	Eu[a]	$4{\cdot}10^{-10}$–10^{-3}	2.0

[a] Ni and Eu reference isotherms. For Pb reference isotherm see Table 1

the lowest blocking element concentration). A summary of the experimental conditions is given in Table 2.

3. Modelling approach with the 2SPNE SC/CE adsorption model

To quantitatively describe the experimental Pb adsorption data and the effect of competitive adsorption on montmorillonite and/or illite, the 2SPNE SC/CE model was used (Bradbury and Baeyens, 1997, 2009a). Briefly, this model describes the adsorption as a combination of CE on the planar sites (PS) and pH dependent SC on the amphoteric surface hydroxyl groups (≡SOH sites) situated at clay platelet edges (Davis and Kent, 1990; Sposito, 1984). The protolysis behaviour of the clay minerals is described by 2 types of weak sites ($\equiv S^{W1}OH$ and $\equiv S^{W2}OH$) having the same site capacity ($40{\cdot}10^{-3}$ mol·kg^{-1}) but different protolysis constants. In addition, a strong type site with high affinity to metal adsorption but with a low capacity ($2{\cdot}10^{-3}$ mol·kg^{-1}) is present and has the same protolysis constants as the $\equiv S^{W1}OH$ sites. The clay specific parameters (i.e., site capacities and protolysis) are fixed in all of the modelling for each clay mineral and are detailed in Table 3. The model was developed without the need for an electrostatic term in the mass action relations used to define protolysis and SC constants. A detailed description of the adsorption model for montmorillonite and illite is given in Bradbury and Baeyens (1997, 2009a).

Table 3
Site capacity values and protolysis reactions and constants for Na-montmorillonite and Na-illite used in the 2SPNE SC/CE adsorption model (Bradbury and Baeyens, 1997, 2009a).

Site type	Na-montmorillonite		Na-illite	
	Capacity			
$\equiv S^{S}OH$	$2.0{\cdot}10^{-3}$ mol·kg^{-1}		2.0 x 10^{-3} mol·kg^{-1}	
$\equiv S^{W1}OH$	$4.0{\cdot}10^{-2}$ mol·kg^{-1}		4.0 x 10^{-2} mol·kg^{-1}	
$\equiv S^{W2}OH$	$4.0{\cdot}10^{-2}$ mol·kg^{-1}		4.0 x 10^{-2} mol·kg^{-1}	
Planar sites (CEC)	0.870 eq·kg^{-1}		0.225 eq·kg^{-1}	
Protolysis reactions	log K			
	$\equiv S^{S/W1}OH$	$\equiv S^{W2}O$-H	$\equiv S^{S/W1}OH$	$\equiv S^{W2}O$-H
$\equiv SOH + H^+ \Leftrightarrow \equiv SOH_2^+$	4.5	6.0	4.0	8.5
$\equiv SOH \Leftrightarrow \equiv SO^- + H^+$	−7.9	−10.5	−6.2	−10.5

Table 4
Aqueous hydrolysis reactions and constants for Pb used in the modelling (Baes and Mesmer, 1976).

Hydrolysis reactions	log K
$Pb^{2+} + H_20 \Leftrightarrow PbOH^+ + H^+$	−7.71
$Pb^{2+} + 2H_20 \Leftrightarrow Pb(OH)_2^0 + 2H^+$	−17.12
$Pb^{2+} + 3H_20 \Leftrightarrow Pb(OH)_3^- + 3H^+$	−28.06

Important parameters in the modelling of the Pb experiments carried out in simple background electrolytes without inorganic/organic ligands are the hydrolysis constants since they are related to the SC constants fitted from the experimental data. The hydrolysis constants for Pb used in the modelling are given in Table 4.

Hydrolysis, selectivity coefficients and SC constants for Ni, Co, Zn and Eu necessary for the modelling of the competition experiments are summarized in Tables SI1 to SI3.

Thermodynamic calculations were performed with the code MINSORB (Bradbury and Baeyens, 1997), which is derived from geochemical code MINEQL (Westall et al., 1976) and which contains subroutines for calculating CE and SC reactions simultaneously.

4. Results and discussion

4.1. Pb adsorption measurements and modelling

4.1.1. Cation exchange of Pb^{2+} and Na^+ on Na-IdP and Na-SWy

The equilibrium data for the displacement of Pb^{2+} by Na^+ can be represented by the following mass action reaction,

$$2\,Na - clay + Pb^{2+} \Leftrightarrow Pb - clay + 2\,Na^+$$

and is defined by the selectivity coefficient, ${}^{Pb}_{Na}K_c$ (Gaines and Thomas, 1953) according to the mass action law,

$${}^{Pb}_{Na}K_c = \frac{N_{Pb}}{N_{Na}^2}\cdot\frac{[Na]^2}{[Pb]}\cdot\frac{(\gamma_{Na})^2}{(\gamma_{Pb})}$$

where N_{Pb} and N_{Na} are the equivalent fractional occupancies, defined as the equivalent of Na (or Pb) adsorbed per kg of clay mineral divided by the cation exchange capacity (CEC) [eq·kg^{-1}]; [Na] and [Pb] are the aqueous molar concentrations (M) and γ_{Na} and γ_{Pb} are aqueous phase activity coefficients.

The ln K_c values for the Pb^{2+}-Na^+ exchange measured on Na-IdP and Na-SWy, as function of the Pb occupancy (N_{Pb}) are plotted in Fig. 1a and b, respectively. The selectivity coefficients are slightly varying as function of the Pb loadings up to N_{Pb} ~0.9, where after an increase of the ln K_c values is observed. Such behaviour has also been observed by Van Bladel and Menzel (1969) for Sr^{2+}-Na^+ exchange on Wyoming bentonite and by Maes et al. (1975) for divalent transition metals on montmorillonite. It should be mentioned that at high N_{Pb} values (i.e., low N_{Na} values) the ln K_c value is sensitive to the CEC value of the given clay mineral. Within the uncertainties of the experimentally determined Cs-CEC (SWy = 870 ± 35 meq·kg^{-1}, IdP = 225 ± 10 meq·kg^{-1}), the curve can be fully flattened or the increase emphasized as shown by the error bands in Fig. 1. It is also known that the CEC for divalent cations is higher than for monovalent cations, which could also influence the K_c calculation at higher Pb^{2+} loadings.

It is of interest to compare the ion exchange data for both clays studied. By graphical integration of the ln K_c composition plots according to $\ln K_{ex} = -1 + \int_0^1 \ln {}^{Pb}_{Na}K_c \, dN_{Pb}$ (Gaines and Thomas, 1953), the values of the exchange constants (K_{ex}) and the corresponding Gibbs free energy (ΔG_{ex} = -RT·ln K_{ex}) can be derived (Table 5).

The value for the Pb^{2+}-Na^+ exchange on montmorillonite is in the range what is commonly found for simple exchange of divalent transition metals (Maes et al., 1975). On the other hand the value of Pb on illite is a factor of ~4 higher compared with montmorillonite. The reason for the more pronounced exchange behaviour for Pb towards illite is not clear. The ${}^{Pb}_{Na}K_c$ values derived above for the CE contribution to the total adsorption of Pb on SWy and IdP are given in Table 6 and were further used as fixed parameters in the modelling of the adsorption edges and isotherms.

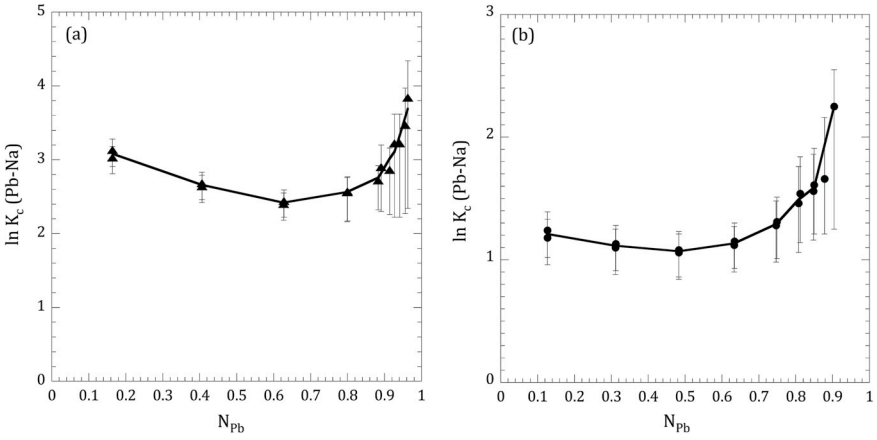

Fig. 1. Natural logarithm of the stoichiometric selectivity coefficient for the Pb^{2+}-Na^{+} exchange against the equivalent fraction of Pb^{2+} on (a) Na-IdP and (b) Na-SWy.

Table 5
Ln K_c, Ln K_{ex} and ΔG_{ex} values (in kJ·mol) for the exchange (25 °C) of Pb^{2+}-Na^{+} on IdP and SWy (total normality 0.011 N).

Clay mineral	$\int_0^1 \ln^{Pb}_{Na} K_c$	ln K_{ex}	ΔG_{ex}
Illite (IdP)	2.7	1.7	−4.2
Montmorillonite (SWy)	1.2	0.2	−0.5

4.1.2. Pb adsorption edges and isotherms on Na-IdP and Na-SWy: experimental data

In order to avoid unnecessary repetition in section 4.1.2 and 4.1.3 the experimental adsorption data are presented in the same graphs together with the modelled curves. Symbols represent the experimental data, continuous lines (black or green) represent the calculated overall adsorption and the coloured broken lines are the contributions of the individual surface species to the total adsorption.

Pb adsorption edges: The results of the adsorption measurements are expressed in terms of solid-liquid distribution ratios (R_d) plotted against pH, with R_d ($L{\cdot}kg^{-1}$) defined as:

$$R_d = \frac{[Me_{init}] - [Me_{eql}]}{[Me_{eql}]} \cdot \frac{V}{m}$$

where $[Me_{init}]$ is total (active + inactive) initial aqueous metal concentration (M), $[Me_{eql}]$ is total (active + inactive) equilibrium aqueous metal concentration (M), V is volume of liquid phase (L), and m is mass of solid phase (kg).

The Pb adsorption edges on Na-IdP and Na-SWy in 0.1 M NaCl shown in Fig. 2a and b, respectively, exhibit the typical shape of pH dependent adsorption as observed for elements such as e.g., Fe^{2+}, Zn^{2+}, Ni^{2+}, Eu^{3+} and $UO_2{}^{2+}$ on clay minerals (Baeyens and Bradbury, 1997; Bradbury and Baeyens, 2009a; Montoya et al., 2018; Schnurr et al., 2015; Soltermann et al., 2014a; Tournassat et al., 2018). At pH < 4 adsorption is comparatively low, and the pH dependency is rather limited whereas above pH ~4 adsorption increases as a function of pH until a plateau is reached. The adsorption of Pb is more pronounced on illite than on montmorillonite over the entire investigated pH range, which is in line with the higher adsorption of Ni and Zn on Na-IdP compared to Na-SWy (Bradbury and Baeyens, 1997, 2009a; Montoya et al., 2018). In the acidic range of the edge (1.5 < pH < 3) the adsorption on Na-IdP varies from log R_d ~2.3–3 $L{\cdot}kg^{-1}$ and increases up to pH ~6 reaching a log R_d plateau value of ~5.8 $L{\cdot}kg^{-1}$. The adsorption of Pb on Na-SWy varies between log R_d values 2–2.3 $L{\cdot}kg^{-1}$ in the pH range 2–4, and increases up to pH ~7.5 attaining a maximum value of log R_d ~5.3 $L{\cdot}kg^{-1}$.

Pb adsorption isotherms are plotted both as the amount of metal adsorbed, $[Me_{ads}]$ expressed in $mol{\cdot}kg^{-1}$ against the metal equilibrium concentration, $[Me_{eql}]$ (M) with

$$[Me_{ads}] = ([Me_{init}] - [Me_{eql}]) \cdot \frac{V}{m}$$

and in terms of R_d plotted against $[Me_{eql}]$. The relation between both is given by

$$R_d = \frac{[Me_{eql}]}{[Me_{ads}]}$$

The reason for this double plotting is on one side the direct comparison of the R_d values at trace concentration for the isotherms with the adsorption edges, whereas the plot $[Me_{ads}]$ vs $[Me_{eql}]$ shows the different site types and their capacities.

Adsorption isotherms measured for Pb on conditioned Na-IdP at pH ~3 (in 0.1 and 0.3 M NaCl), at pH ~6 (in 0.02 M NaCl) and at pH ~7 (in 0.1 M NaCl under N_2 and atmospheric air conditions) and on Na-SWy in 0.1 M NaCl at pH ~6 and ~7 are presented in Figs. 3 and 4, respectively.

All the isotherms measured on both clay minerals exhibit an overall non-linear behaviour. At low $[Pb_{eql}]$ the adsorption is linear (Langmuir type, slope equal 1) with increasing concentration the adsorption becomes non-linear and exhibits a Freundlich-type behaviour (slope < 1). The non-linearity of the isotherms measured at pH values where adsorption becomes pH dependent (see Fig. 2) follows the expected concentration dependency and complies with the adsorption on at least two different site types (i.e., PS, $\equiv^{S}SOH$ and/or $\equiv^{W1}SOH$). Experimental data obtained at trace $[Pb_{eql}]$ for both clay minerals agree within ± 0.3 log units well with the Pb adsorption edge data at the corresponding pH values, confirming the consistency of the data. Striking is the minor decrease of ~0.2 log units of the log R_d value of trace Pb at pH ~3 on Na-IdP in 0.3 M NaCl compared to the adsorption in 0.1 NaCl (Figs. 3a–1 and 3b-1). If one assumes CE being the prevailing uptake mechanism at pH ~3, CE contribution should decrease by approx. one order of magnitude in 0.3 M NaCl, and hence, should lead to a larger decrease of the log R_d values as observed in Figs. 3a–1 and b-1. The good agreement between the isotherms measured on Na-IdP at pH ~7 under N_2 and under atmospheric conditions (Fig. 3d) indicate that no quantifiable precipitation of $PbCO_3$ or $Pb_3(CO_3)_2(OH)_2$ occurred at the highest Pb concentrations.

4.1.3. Pb adsorption edges and isotherms on Na-IdP and Na-SWy: modelling

To increase the robustness of adsorption modelling, more than one

set of experimental data must be reproducible with the same set of parameters. Both types of data sets, adsorption edges and isotherms were modelled using the aqueous Pb hydrolysis constants (Table 4), the non-adjustable clay mineral specific parameters (Table 3) and the $^{Pb}_{Na}K_c$ values on the planar sites for Na-SWy and Na-IdP derived from the Pb^{2+}-Na^+ exchange experiments (Table 6). The only adjustable parameters to reproduce the adsorption edges and isotherms were the SC constants for Pb on the strong and weak sites. The modelling of the edges and the isotherms was carried out in an iterative way until the best fit to all adsorption data sets was achieved.

Na-IdP: The green continuous curve in Fig. 2a is the best fit by eye to the experimental adsorption edge data by using the Pb^{2+}-Na^+ selectivity coefficient for CE on the PS and two SC reactions and corresponding constants on the strong sites (Table 6). The fit obtained with these parameters describes well the adsorption edge above pH 5, whereas the data are underpredicted (up to ~0.6 log units) in the low pH range. Increasing the first SC constant to reproduce the data in the acidic range, however, would result in a much larger overestimation of the adsorption in the pH range 6–9 (~2 orders of magnitude), see e.g., Bradbury and Baeyens (1997). Consequently, the two SC reactions and corresponding SC constants describing correctly the edge rise and plateau values ($\equiv^S SOPb^+$ and $\equiv^S SOPbOH^0$, broken red lines in Fig. 2a) were retained as the most appropriate and were used in the following modelling steps.

Assuming CE on the PS to model the non-linear adsorption isotherms measured at pH ~3 in 0.1 M and 0.3 M NaCl (Fig. 3a and b) (green curves in Fig. 2a and b) reproduces well both isotherms in the higher concentration range ($[Pb_{eql}] > 10^{-5}$ M) and consequently confirms the correctness of the selectivity coefficient derived in the previous CE experiments (see section 4.1.1). However, the experimental data at $[Pb_{eql}] < 10^{-5}$ M, are underpredicted in both cases, which supports the anomalous adsorption behaviour in the low pH range in Fig. 2a. The low pH-trace Pb concentration data (edge and the two isotherms) could only be fully reproduced (black curve in Figs. 2a, 3a and 3b) by considering a new site denoted as "high affinity site" (HAS) (capacity, associated SC reaction and log ^{HAS}K are given in Table 6). The Langmuir type regions describing the concentration dependent contributions of Pb adsorption on the three different sites (strong, HAS, PS) to the overall uptake of Pb on Na-IdP are illustrated in the isotherms at pH ~3. The necessity to introduce an additional site type to quantitatively describe adsorption in the acid range on Na-IdP is also supported by the study of Montoya et al. (2018). Similar to Pb in the present study, trace Zn at low pH showed anomalous high adsorption which did not follow the ionic strength dependency and could not be modelled solely with CE on the PS. It should be emphasized that the HAS are necessary to fully reproduce the experimental data but nothing is known about their physical nature (e.g., clay surface site, mineral impurity). Also its relevance is limited in natural environments (pH < 4).

A very good fit of the adsorption isotherms measured at pH ~6 in 0.02 M NaCl and at pH ~7 in 0.1 M NaCl was obtained by considering the SC reactions on the strong sites derived from the pH dependent data and the formation of an additional Pb surface complex on the weak sites ($\equiv^{W1} SOPb^+$). Besides pH and concentration dependency the model also describes the influence of ionic strength (0.1 M, 0.3 M and 0.02 M).

Na-SWy: To model the adsorption data on Na-SWy a similar procedure as for Na-IdP was applied. In contrast to illite, adsorption at pH ≤ 4 and trace Pb could be fairly well described by considering only the CE reaction on the planar sites with the selectivity coefficient of 3.3 (see section 4.1.1 and Table 6). HAS as in the case of IdP were not necessary.

The pH dependent part of the adsorption edge is well reproduced (even so the data scatter is more pronounced than in case of Na-IdP) by considering the formation of two Pb surface complexes on the strong sites, $\equiv^S SOPb^+$ and $\equiv^S SOPbOH^0$, similar to illite, but with weaker SC constants. Keeping these reactions and constants fixed, allowed to obtain a first approximate fit of the non-linear part of the adsorption isotherms by considering an additional SC reaction on the weak sites ($\equiv^{W1} SOPb^+$). Refined values for all the SC constants were finally obtained by the iterative fit of both types of experimental data. The model slightly underpredicts the adsorption data obtained for the isotherms at trace Pb concentrations by ~0.2 log units at pH ~6 and ~0.5 log units at pH ~7, which is a consequence of the fit optimization of the comparatively scattered adsorption edge data. To summarize, for both clay minerals a good correspondence between modelled curves and measured Pb adsorption edge and isotherm data was achieved with the adsorption reactions and corresponding constants summarized in Table 6.

Table 6
Summary of the Pb SC reactions and constants on strong ($\equiv S^SOH$), weak ($\equiv S^{W1}OH$) and high affinity (HAS) sites and selectivity coefficients for Na^+-Pb^{2+} exchange on PS for montmorillonite and illite determined in this study.

	SWy	IdP
SC reactions on strong sites	**log ^SK**	
$\equiv^S SOH + Pb^{2+} \equiv^S SOPb^+ + H^+$	1.0	2.7
$\equiv^S SOH + Pb^{2+} + H_20 \equiv^S SOPbOH^0 + 2H^+$	−7.6	−5.3
SC reaction on weak sites	**log ^{W1}K**	
$\equiv^{W1} SOH + Pb^{2+} \equiv^{W1} SOPb^+ + H^+$	−1.5	0.3
SC reaction on high affinity sites (capacity $2 \cdot 10^{-4}$ mol·kg^{-1})	**log ^{HAS}K**	
$> HAS + Pb^{2+} > HAS\text{-}Pb^{2+}$	–	6.5
CE selectivity coefficients for PS	**K_c**	
$2Na\text{-}PS + Pb^{2+}$ Pb-PS $+ 2Na^+$	3.3	14.8
$Na\text{-}PS + H^+$ H-PS $+ Na^+$	1.0[a]	1.0[a]

[a] Taken from Gilbert and Laudelout (1965)

4.2. Competitive adsorption: experimental and modelling

In this section the experimental and modelling results of the competitive adsorption study in 0.1 M NaCl at pH ~7 involving binary combinations of Pb and Ni, Zn, Co or Eu on Na-IdP are presented and discussed. Adsorption experiments were performed in which one metal was present at very low concentration (trace element) and the other metal at increasing concentration (blocking element). When both elements are competitive it is expected that the adsorption of blocking element progressively fills up the strong sites and thereby reduces or even impedes the adsorption of the trace metal on these sites, resulting in a progressive decrease of the R_d value with adsorption of the trace element only on the weak and CE sites.

If both metals are non-competitive the R_d value of the trace element should remain unchanged independently of the increasing blocking element concentration. Whether elements are fully or partially competing was verified by using the 2SPNE SC/CE model for illite and the model parameters for the elements involved (i.e., hydrolysis, SC reactions/constants, selectivity coefficients for Pb (Tables 3, 4 and 6) and Ni, Zn, Co or Eu in Tables SI1, SI2 and SI3) (section 4.2.3). The experimental R_d values of the trace elements (black symbols) are plotted at the blocking Me_{eql} concentrations in the graphical representations. Blue curves illustrate the modelling results of the adsorption of the trace metal under the assumption that the pairs of elements are mutually competitive, *i.e.,* they sorb on the same strong sites and the adsorption value of the trace element is governed by the concentration of the

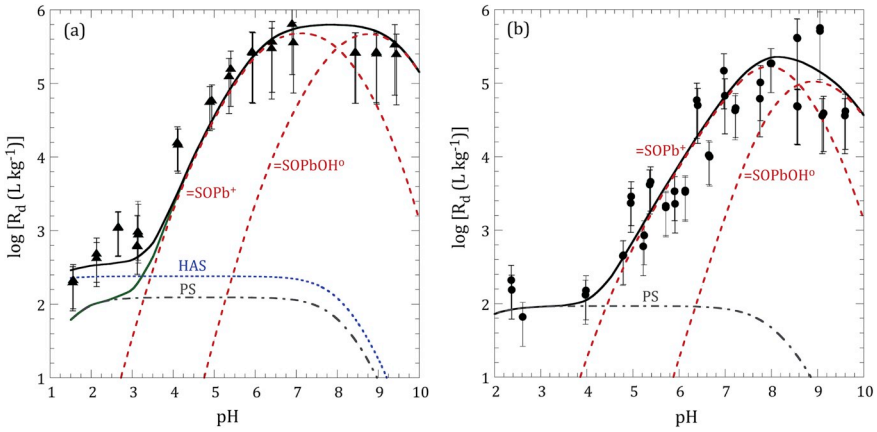

Fig. 2. Pb adsorption edges in 0.1 M NaCl (a) on Na-IdP and (b) on Na-SWy.

blocking element and the difference of the SC constants of the respective metals. In the case the pairs of elements are not competing (i.e., they sorb on different strong sites), the adsorption value of the trace element is not affected by the blocking element and remains constant over the entire concentration range, as indicated by the red lines. This presentation allows to judge whether Pb and Ni, Co, Zn or Eu are competing for the same adsorption sites or not and to which extend.

4.2.1. Trace Ni, Co, Zn, Eu/blocking Pb on Na-IdP

The Pb isotherm on Na-IdP shown in Fig. 3d (open symbols) is the reference isotherm for the competitive adsorption measurements with Pb as blocking element. Fig. 5a, b, c and d show the measured and predicted (assuming full or non-competition) adsorption behaviour of trace Ni, Co, Zn and Eu, respectively, in the presence of increasing Pb concentrations.

In the case of Ni, the adsorption values decrease from ~4.1 to ~3 $L \cdot kg^{-1}$ with increasing Pb_{eql} concentration (Fig. 5a) suggesting that both elements are to a certain extend competitive. Under the assumption that trace Ni and Pb are competitive, the Ni adsorption should follow the blue curve and decrease to log R_d ~1.8 $L \cdot kg^{-1}$ at the highest Pb_{eql} concentration. However, the less pronounced decrease compared to the modelled curve for $[Pb_{eql}] > 10^{-8}$ M, indicates that trace Ni and Pb only partially compete (i.e., a fraction of the trace Ni concentration still has access to the strong sites despite the high concentration of the blocking element). Note that the trace Ni adsorption values at trace Pb concentration for this particular Na-IdP batch are slightly higher than the data published in the open literature, however, are within the observed data scatter (e.g., Baeyens and Bradbury, 1997; Bradbury and Baeyens, 2009a). To model the present data, the constant for the first Ni surface complex ($\equiv S^SONi^+$) was increased by 0.3 log units (i.e., log K = 1.0, see Table SI2). The variability of the SC constant illustrates the uncertainties/scatter of the experimental data and adjusting this constant has no effect on the quantification of the degree of competitiveness.

The adsorption behaviour of trace Co as a function of increasing Pb concentration (Fig. 5b) is very similar to Ni and clearly suggests partial competition. Trace Co adsorption data obtained in this study are slightly higher than the data given in Montoya et al. (2018) and similar to Ni the first Co surface complex ($\equiv S^SOCo^+$) was adjusted to log K_1 = 1.6 to fit this particular data set (see Table SI2).

More striking is the behaviour of trace Zn (Fig. 5c), which appears not to be affected by the increasing Pb concentration, indicating that trace Zn and Pb do not compete.

In the case of Eu (Fig. 5d), no conclusive statement can be made. The decrease of measured adsorption values is less pronounced than in the modelled curve, which would suggest that trace Eu and Pb are partially competing. However, one could also argue that the measured data somehow follows the shape of the modelled curve and that within the experimental error bars modelled curve and experimental data are close, suggesting that trace Eu and Pb are competing for the same type of strong sites. Despite the uncertainty the modelling was made assuming partial competiveness in section 4.2.3.

4.2.2. Trace Pb/blocking Ni/Eu on Na-IdP

The competitive behaviour of trace Pb in the presence of blocking Ni and Eu on Na-IdP is illustrated in Fig. 6. The Ni and Eu reference adsorption isotherms determined simultaneously with the competitive adsorption experiments, together with the SC reactions and constants used to model both isotherms, are given in the SI. The experiment with blocking Zn was not performed. The outcome of these experiments is rather surprising. In both cases the adsorption of trace Pb remains constant with increasing blocking element concentration, suggesting that trace Pb is neither competing with blocking Ni nor with blocking Eu. Trace Ni or Eu with blocking Pb (Fig. 5a and d) or vice versa trace Pb with blocking Ni or Eu (Fig. 6) clearly yield different results. In the former, the metals are partially competitive whereas in the latter the metals behave as being non-competitive. The R_d values obtained for trace Pb in the presence of $[Eu_{eql}] < 10^{-8}$ M (Fig. 6b) are slightly lower than in the Pb/Ni system (Fig. 6a) and as determined in the pure Pb/Na-IdP system, however are within scattering range (and error bars) of the measurements (see Fig. 3d).

Soltermann et al. (2014b) made similar observations when investigating the competitive adsorption of Zn and Fe^{II} on an iron free synthetic montmorillonite. Zn and Fe^{II} were fully competitive for the strong sites in case Fe^{II} is the blocking element, whereas the adsorption of trace Fe^{II} was not affected by increasing Zn concentration. However this different adsorption behaviour was explained by the existence of sorption sites with higher affinity for Fe^{III} and where surface-induced oxidation of the sorbed Fe^{II} to Fe^{III} occurred, and which were not accessible for Zn.

The reasons for these contradicting results are currently not understood and cannot be solved in the context of the present study based on macroscopic experiments and thermodynamic modelling.

4.2.3. Quantification of competitive adsorption

Non-competitive adsorption: The results presented above have

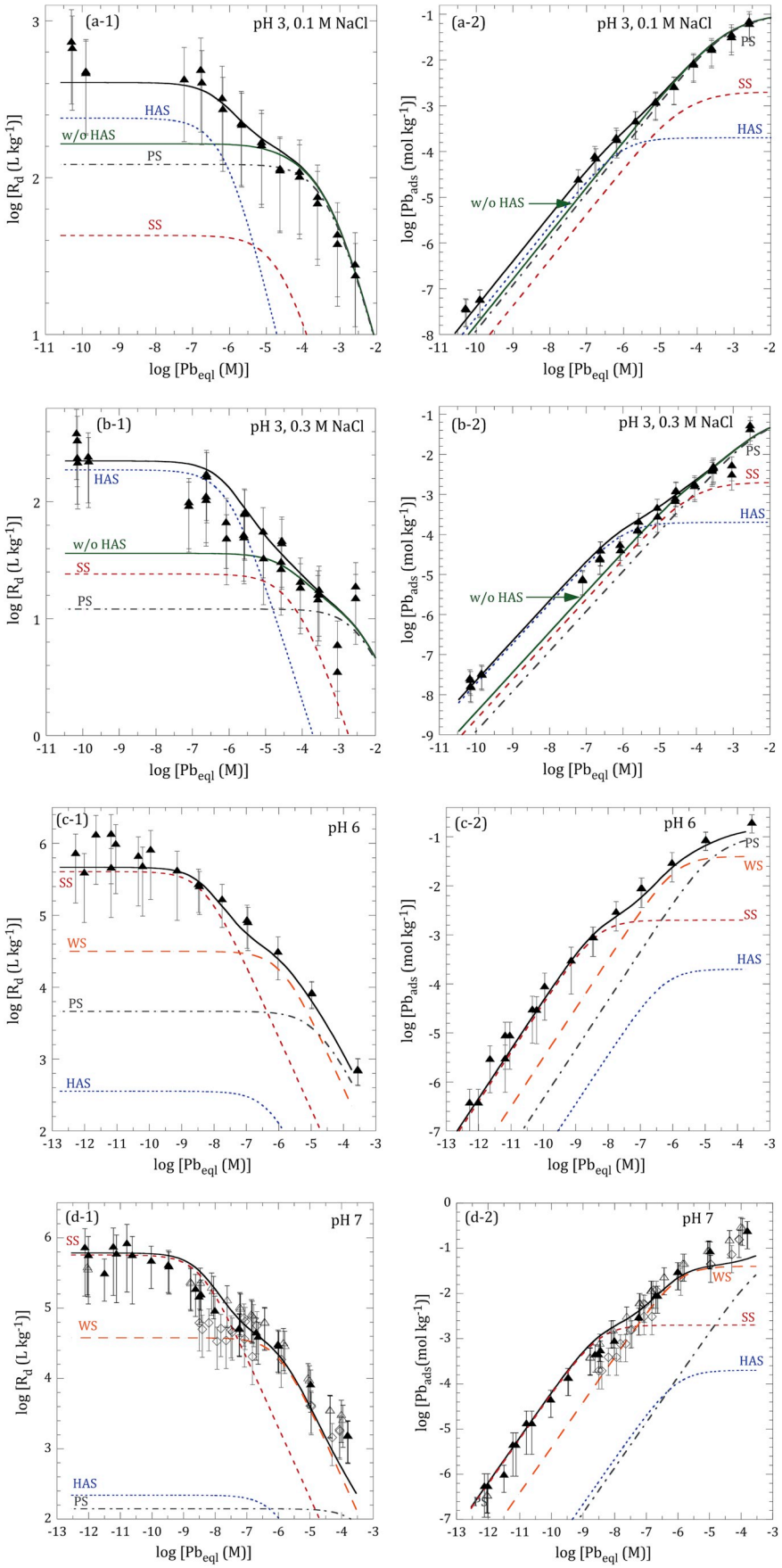

Fig. 3. Adsorption isotherms for Pb on Na-IdP (a-1, a-2) at pH ~3 in 0.1 NaCl, (b-1, b-2) at pH ~3 in 0.3 M NaCl, (c-1, c-2) at pH ~6 in 0.02 M NaCl and (d-1, d-2) at pH ~7 in 0.1 M NaCl (closed symbols in N_2 atmosphere, open symbols in air atmosphere).

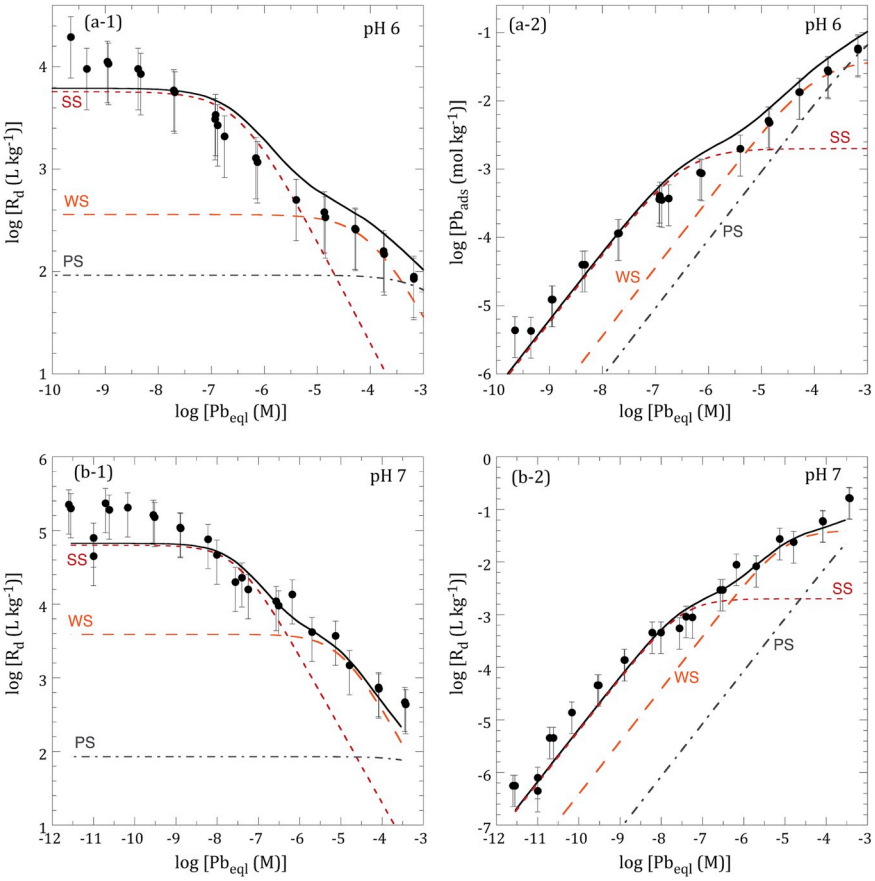

Fig. 4. Adsorption isotherms for Pb on Na-SWy in 0.1 M NaCl at pH ~6 (a-1, a-2) and at pH ~7 (b-1, b-2).

shown non-competitive adsorption behaviour for the Zn/Pb, Pb/Ni and Pb/Eu systems, where the former metal is present at trace concentration and the latter as blocking element. This process cannot be quantitatively described with the 2SPNE SC/CE adsorption model in its present form since only one set of strong sites (capacity of 2 mmol·kg^{-1}) accessible to all metals, is defined in the model, and hence competitive adsorption is intrinsically assumed. In order to reproduce the non-competitiveness, additional metal specific sets of strong sites (with the same protolysis constants and site capacity) must be included in the model. These sites can be considered as sub sets of weak sites which exhibit the same protolysis behaviour (Bradbury and Baeyens, 2005a).

Partially competitive adsorption: For the cases where partial competition is experimentally observed (e.g., Fig. 5a, b and 5d) the data can be modelled by assuming that a given fraction of the strong sites is accessible only to the trace element and on the remaining fraction both trace and blocking element do adsorb according to their respective SC constants. The modelling of trace metal (Me = Ni, Co or Eu) adsorption in these experiments was carried out as follows. In the batch experiments the trace metals are present at a fixed inventory, a fixed *S* (see Table 2) and with varying initial Pb concentrations. For each individual data point the log R_d value is experimentally determined and with the known initial concentration ([Me_{in}]), the final concentration ([Me_{eql}]) can be calculated. Since the trace Me R_d values in such a system are linked to the [Me_{eql}], a single curve is obtained from the data analyses (both experimentally and modelling). In Fig. 7 the experimental data are plotted as log R_d versus [Me_{eql}]. In a first calculation the data are modelled assuming that both metals are mutually competitive. This is illustrated by the blue curves in Fig. 7. The experimental R_d values are, however, higher than the calculated values (differences are indicated by the red arrows in Fig. 7 and correspond to ~1.6, 1 and 0.6 log unit(s) for Ni, Co and Eu, respectively). The modelling was repeated under the constraint that a given fitted fraction of the strong sites is non-competitive (solid red curves) and indicate that in the case of Ni (Fig. 7a) 10% of the strong sites are required to reproduce the experimental data. For Co (Fig. 7b) and Eu (Fig. 7c) 3% and 10% of non-competitive strong sites are required, respectively, as indicated by the solid red curves. The uncertainty on these fitted values based on a maximum uncertainty of 60% on the experimentally determined R_d values, is given in the respective figure for the data point at the highest blocking element concentration (black bars perpendicular to the curves). As already discussed in section 4.2.1, the degree of partial competition for Eu is not clearly evidenced (see Fig. 7c). The outcome of the partial competition modelling is that for the conditions under which these experiments were performed (i.e., simultaneously addition of trace and blocking element, reaction time 1 week) approximately 3–10% of the strong sites could be considered to be non-competitive whereas 90–97% of the strong sites remain competitive.

5. Conclusions

In order to assess the safety of radioactive waste repositories or the risk associated to contaminated natural environments (e.g., soils, subsurface waters), a fundamental understanding of the uptake processes of (radio-) contaminants onto relevant components of soils and

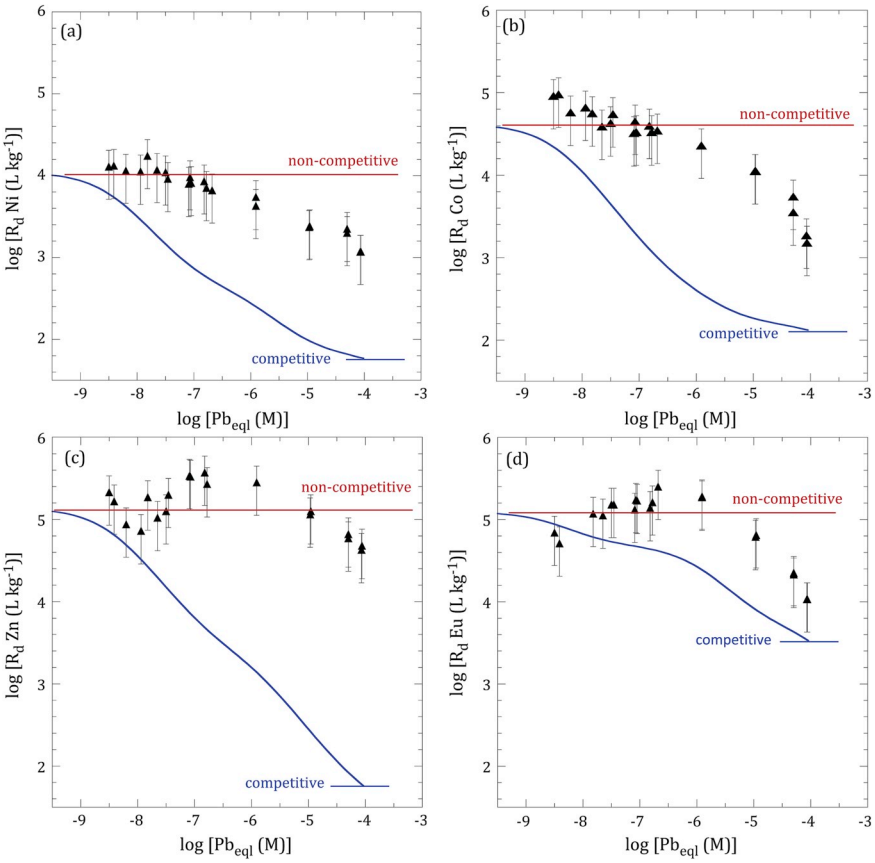

Fig. 5. Competitive adsorption experiments with Pb as blocking element in the presence trace concentrations of (a) Ni, (b) Co, (c) Zn and (d) Eu on Na-IdP in 0.1 M NaCl at pH ~ 7.

sediments which affect their mobility is of utmost importance. In the present study, the focus was on clays minerals as major reactive constituents of soils and sediments.

The adsorption of divalent lead, an environmental relevant heavy metal, onto illite and montmorillonite was thoroughly investigated. The measurements obtained over a wide range of experimental conditions allowed quantifying the adsorption (R_d values), and, by modelling all the data, to extend the 2SPNE SC/CE model with CE selectivity coefficients and SC constants for Pb on both clay minerals. The anomalous high adsorption of trace Pb in the acidic region observed on Na-IdP could be modelled by introducing a pH and ionic strength independent adsorption reaction on a new site type exhibiting a very small capacity but a very high adsorption constant.

Competitive adsorption on illite was measured in binary metal systems and the degree of competitiveness could be quantitatively described with a modified 2SPNE SC/CE model. Especially in the framework of the safety analysis of radioactive waste repositories, verifying and quantifying (if necessary) the potential influence of competitive adsorption on the retention of radionuclides in the near- and far-fields through the presence of high concentrations of stable elements is highly relevant. The results obtained suggest that competitive adsorption is not a straightforward process and raise further questions. The adsorption behaviour of trace Co, Ni and Eu on illite when Pb is present at high concentrations reveals that these metals are partially competing for the strong edge sites, whereas the reciprocal experiments indicate that trace Pb is not competing with blocking Ni or Eu. Trace Zn appears to be non-competitive in the presence of blocking Pb. To understand these results and to improve the mechanistic comprehension of competitive adsorption reactions on clay minerals further investigations and particularly the application of complementary structure sensitive methods are required. On the one hand, aspects such as long-time kinetics or/and higher trace metal inventory effects should be addressed macroscopically. On the other hand, a detailed molecular scale understanding of the adsorption mechanisms of the different elements (e.g., location and nature of the metal complexes on the clay surface) is indispensable. Particularly, for some divalent elements, it is not clear which mechanism controls the retention at trace concentration (adsorption or substitution) and consequently how this could affect the competitive adsorption behaviour (Tournassat et al., 2013). The use of XAS supported by molecular modelling techniques (Churakov and Dähn, 2012; Dähn et al., 2011) could help to unravel structural environment of the different surface complexes, provided there are no intrinsic XAS related difficulties (e.g., nature/coordination chemistry of the metal, metal loading, interference from the clay structure).

Finally, the implementation of exhaustive thermodynamic law-of-mass-action adsorption models such as the 2SPNE SC/CE model in reactive transport codes will enable the calculation of the speciation of (radio)contaminants in natural environments with complex geochemistry (e.g., mineralogy, interstitial porewater composition), and hence, improve the reliable prediction of the migration behaviour of Pb in the geo- and biosphere.

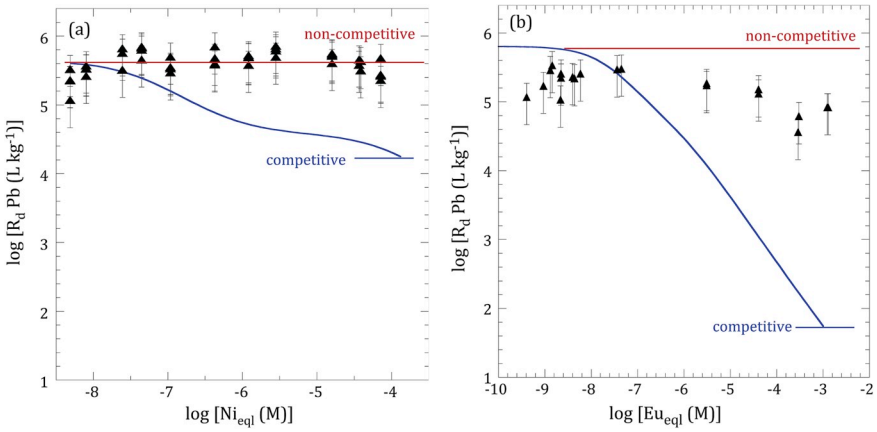

Fig. 6. Competitive adsorption of trace Pb in the presence of increasing (a) Ni concentrations and (b) Eu concentrations on Na-IdP in 0.1 M NaCl at pH ~ 7.

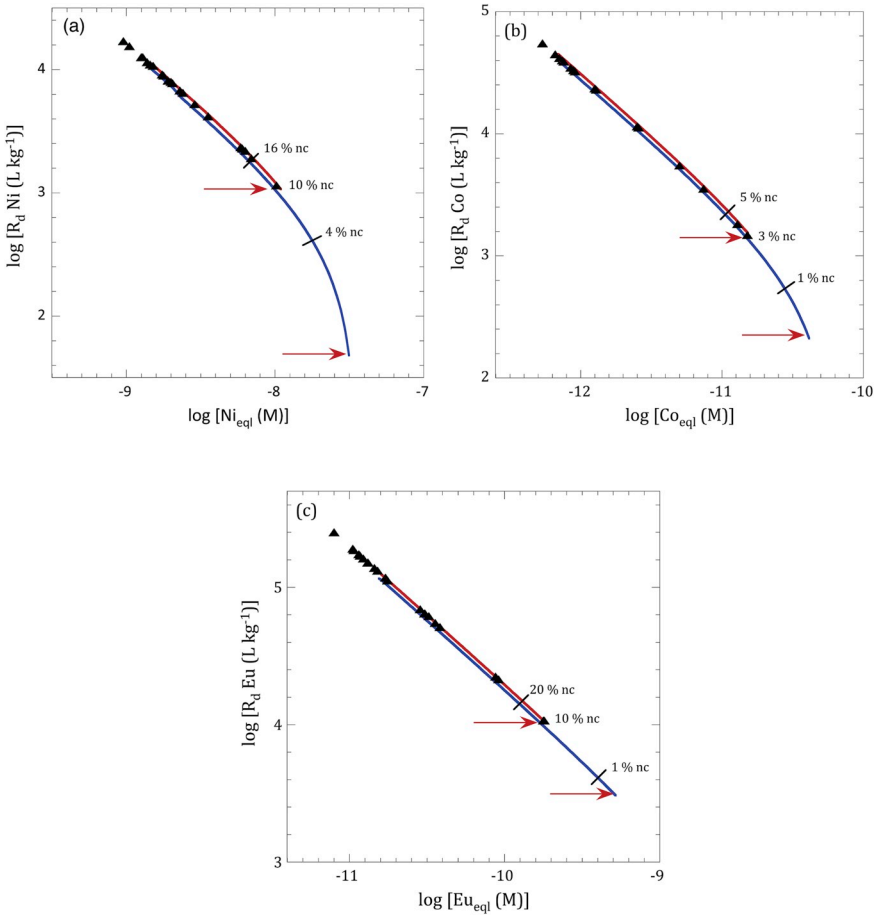

Fig. 7. Modelling partial competitive adsorption of (a) Ni, (b) Co and (c) Eu on Na-IdP as a function of increasing Pb concentrations in 0.1 M NaCl at pH ~ 7. Black bars perpendicular to the curves, indicate the uncertainties on the quantification.

Acknowledgements

A. Schaible and E. Eltayeb carried out much of the experimental work and their contributions to this study are gratefully acknowledged. Partial financial support was provided by the National Cooperative for the Disposal of Radioactive Waste (Nagra), Wettingen, Switzerland.

Appendix A. Supplementary data

Supplementary data to this article can be found online at https://doi.org/10.1016/j.apgeochem.2018.11.005.

References

Akafia, M.M., Reich, T.J., Koretsky, C.M., 2011. Assessing Cd, Co, Cu, Ni, and Pb Sorption on montmorillonite using surface complexation models. Appl. Geochem. 26, S154–S157.

Altmann, S., 2008. 'Geo'chemical research: a key building block for nuclear waste disposal safety cases. J. Contam. Hydrol. 102, 174–179.

Andra, 2001. Référentiel géologique du site de Meuse/Haute Marne. Rapp. A RP ADS 99-005 de l'Agence nationale pour la gestion des déchets radioactifs. Châtenay-Malabry, France.

Atanassova, I., 1999. Competitive effect of copper, zinc, cadmium and nickel on ion adsorption and desorption by soil clays. Water Air Soil Pollut. 113, 115–125.

ATSDR, 2007. Toxicological Profile for Lead. U.S. Agency for Toxic Substances and Disease Registry, Department of Health and Human Services, Public Health Service, Atlanta, GA.

Baes, C.F., Mesmer, R.E., 1976. The Hydrolysis of Cations. John Wiley & Sons Inc.

Baeyens, B., Bradbury, M.H., 1997. A mechanistic description of Ni and Zn sorption on Na- montmorillonite. 1. Titration and sorption measurements. J. Contam. Hydrol. 27, 199–222.

Baeyens, B., Bradbury, M.H., 2004. Cation exchange capacity measurements on illite using the sodium and cesium isotope dilution technique: effects of the index cation, electrolyte concentration and competition: Modeling. Clay Clay Miner. 52, 421–431.

Barbier, F., Duc, G., Petit-Ramel, M., 2000. Adsorption of lead and cadmium ions from aqueous solution to the montmorillonite/water interface. Colloid. Surface. Physicochem. Eng. Aspect. 166, 153–159.

Bergaya, F., Lagaly, G., 2013. Chapter 1 - general introduction: clays, clay minerals, and clay science. In: Bergaya, F., Lagaly, G. (Eds.), Developments in Clay Science. Elsevier, pp. 1–19.

Bittel, J.E., Miller, R.J., 1974. Lead, cadmium and calcium selectivity coefficients on a montmorillonite, illite and kaolinite. J. Environ. Qual. 3.

Borisover, M., Davis, J.A., 2015. Chapter 2 - adsorption of inorganic and organic solutes by clay minerals. In: Tournassat, C., Steefel, C.I., Bourg, I.C., Bergaya, F. (Eds.), Developments in Clay Science. Elsevier, pp. 33–70.

Bradbury, M.H., Baeyens, B., 1997. A mechanistic description of Ni and Zn sorption on Na- montmorillonite. 2. Modelling. J. Contam. Hydrol. 27, 223–248.

Bradbury, M.H., Baeyens, B., 2005a. Experimental measurements and modeling of sorption competition on montmorillonite. Geochem. Cosmochim. Acta 69, 4187–4197.

Bradbury, M.H., Baeyens, B., 2005b. Modelling the sorption of Mn(II), Co(II), Ni(II), Zn (II), Cd(II), Eu(III), Am(III), Sn(IV), Th(IV), Np(V) and U(VI) on montmorillonite: linear free energy relationships and estimates of surface binding constants for some selected heavy metals and actinides. Geochem. Cosmochim. Acta 69, 875–892.

Bradbury, M.H., Baeyens, B., 2009a. Sorption modelling on illite Part I: titration measurements and the sorption of Ni, Co, Eu and Sn. Geochem. Cosmochim. Acta 73, 990–1003.

Bradbury, M.H., Baeyens, B., 2009b. Sorption modelling on illite. Part II: actinide sorption and linear free energy relationships. Geochem. Cosmochim. Acta 73, 1004–1013.

Breen, C., Bejarano-Bravo, C.M., Madrid, L., Thompson, G., Mann, B.E., 1999. Na/Pb, Na/Cd and Pb/Cd exchange on a low iron Texas bentonite in the presence of competing H + ion. Colloid. Surface. Physicochem. Eng. Aspect. 155, 211–219.

Churakov, S.V., Dähn, R., 2012. Zinc adsorption on clays inferred from atomistic simulations and EXAFS spectroscopy. Environ. Sci. Technol. 46, 5713–5719.

Coles, C.A., Yong, R.N., 2002. Aspects of kaolinite characterization and retention of Pb and Cd. Appl. Clay Sci. 22, 39–45.

Dähn, R., Baeyens, B., Bradbury, M.H., 2011. Investigation of the different binding edge sites for Zn on montmorillonite using P-EXAFS - the strong/weak site concept in the 2SPNE SC/CE sorption model. Geochem. Cosmochim. Acta 75, 5154–5168.

Davis, J.A., Kent, D.B., 1990. Surface complexation modeling in aqueous geochemistry. In: Hochella, M.F., White, A.F. (Eds.), Mineral-water Interface Geochemistry. Mineralogical Society of America, pp. 177–260.

Dixon, J.B., 1991. Roles of clays in soils. Appl. Clay Sci. 5, 489–503.

Donat, R., Akdogan, A., Erdem, E., Cetisli, H., 2005. Thermodynamics of Pb2+ and Ni2+ adsorption onto natural bentonite from aqueous solutions. J. Colloid Interface Sci. 286, 43–52.

Farrah, H.,F., Pickering, W., 1977. The Sorption of Lead and Cadmium by Clay Minerals.

Gabis, V., 1958. Etude préliminaire des argiles oligocènes du Puy-en-Velay (Haute-Loire). Bull. Soc. Franç. Minéral. Cristallog 81, 183–185.

Gaines, G.L.J., Thomas, H.C., 1953. Adsorption studies on clay minerals. II. A formulation of the thermodynamics of exchange adsorption. J. Chem. Phys. 21, 714.

Gilbert, M., Laudelout, H., 1965. Exchange properties of hydrogen ions in clays. Soil Sci. 100, 157–162.

Gräfe, M., Singh, B., Balasubramanian, M., 2007. Surface speciation of Cd(II) and Pb(II) on kaolinite by XAFS spectroscopy. J. Colloid Interface Sci. 315, 21–32.

Groenenberg, J.E., Lofts, S., 2014. The use of assemblage models to describe trace element partitioning, speciation, and fate: a review. Environ. Toxicol. Chem. 33, 2181–2196.

Gu, X., Evans, L.J., Barabash, S.J., 2010. Modeling the adsorption of Cd (II), Cu (II), Ni (II), Pb (II) and Zn (II) onto montmorillonite. Geochem. Cosmochim. Acta 74, 5718–5728.

Hefne, J.A., Mekhemer, W.K., Alandis, N.M., Aldayel, O.A., Alajyan, T., 2008. Kinetic and thermodynamic study of the adsorption of pb (II) from aqueous solution to the natural and treated bentonite. Int. J. Phys. Sci. 3, 281–288.

Helios-Rybicka, E., Wójcik, R., 2012. Competitive sorption/desorption of Zn, Cd, Pb, Ni, Cu, and Cr by clay-bearing mining wastes. Appl. Clay Sci. 65–66, 6–13.

Hizal, J., Apak, R., 2006. Modeling of copper(II) and lead(II) adsorption on kaolinite-based clay minerals individually and in the presence of humic acid. J. Colloid Interface Sci. 295, 1–13.

IPCS, 1977. Lead, Environmental Health Criteria 3. World Health Organization, International Programme on Chemical Safety, Geneva.

IPCS, 1989a. Lead-environmental Aspects, Environmental Health Criteria 85. World Health Organization, International Programme on Chemical Safety, Geneva.

IPCS, 1989b. Mercury-environmental Aspects, Environmental Health Criteria 86. World Health Organization, International Programme on Chemical Safety, Geneva.

IPCS, 1991. Inorganic Mercury, Environmental Health Criteria 118. World Health Organization, International Programme on Chemical Safety, Geneva.

IPCS, 1992a. Cadmium, Environmental Health Criteria 134. World Health Organization, International Programme on Chemical Safety, Geneva.

IPCS, 1992b. Cadmium-environmental Aspects, Environmental Health Criteria 135. World Health Organization, International Programme on Chemical Safety, Geneva.

IPCS, 1995. Inorganic Lead, Environmental Health Criteria 165. World Health Organization, International Programme on Chemical Safety, Geneva.

IPCS, 2001. Arsenic and Arsenic Compounds, second ed. Environmental Health Criteria, vol. 224 World Health Organization, International Programme on Chemical Safety, Geneva.

Li, Z., Tang, L., Zheng, Y., Tian, D., Su, M., Zhang, F., Ma, S., Hu, S., 2017. Characterizing the mechanisms of lead immobilization via bioapatite and various clay minerals. ACS Earth and Space Chemistry 1, 152–157.

Maes, A., Peigneur, P., Cremers, A., 1975. Thermodynamics of transition metal ion exchange in montmorillonite. Proc. Int. Clay Conf. 319–333.

Majone, M., Papini, M.P., Rolle, E., 1993. Clay adsorption of lead from landfill leachate. Environ. Technol. 14, 629–638.

Majone, M., Papini, M.P., Rolle, E., 1996. Modeling lead adsorption on clays by models with and without electrostatic terms. J. Colloid Interface Sci. 179, 412–425.

Manceau, A., Boisset, M.-C., Sarret, G., Hazemann, J.-L., Mench, M., Cambier, P., Prost, R., 1996. Direct determination of lead speciation in contaminated soils by EXAFS spectroscopy. Environ. Sci. Technol. 30, 1540–1552.

Mhamdi, M., Galai, H., Mnasri, N., Elaloui, E., Trabelsi-Ayadi, M., 2013. Adsorption of lead onto smectite from aqueous solution. Environ. Sci. Pollut. Control Ser. 20, 1686–1697.

Montoya, V., Baeyens, B., Glaus, M.A., Kupcik, T., Marques Fernandes, M., Van Laer, L., Bruggeman, C., Maes, N., Schäfer, T., 2018. Sorption of Sr, Co and Zn on illite: batch experiments and modelling including Co in-diffusion measurements on compacted samples. Geochem. Cosmochim. Acta 223, 1–20.

Nagra, 2002. Project Opalinus Clay: Safety Report. Demonstration of Disposal Feasibility (Entsorgungsnachweis) for Spent Fuel, Vitrified High-Level Waste and Long-Lived Intermediate-Level Waste. Technical Report NTB 02–05. Nagra, Wettingen, Switzerland.

Nagra, 2014. Modellhaftes Inventar für radioaktive Materialien MIRAM 14. Technischer Bericht NTB 14-04. Nagra, Wettingen, Switzerland.

OECD/NEA, 2012. Thermodynamic Sorption Modelling in Support of Radioactive Waste Disposal Safety Cases: NEA Sorption Project Phase III. OECD Publishing, Paris.

Ondraf, 2001. SAFIR 2: Safety Assessment and Feasibility Interim Report 2. NIROND-2001-06 E. Ondraf, Brussels, Belgium.

Oubagaranadin, J.U.K., Murthy, Z.V.P., 2009. Adsorption of divalent lead on a Montmorillonite−Illite type of clay. Ind. Eng. Chem. Res. 48, 10627–10636.

Ozdes, D., Duran, C., Senturk, H.B., 2011. Adsorptive removal of Cd(II) and Pb(II) ions from aqueous solutions by using Turkish illitic clay. J. Environ. Manag. 92, 3082–3090.

Payne, T.E., Brendler, V., Ochs, M., Baeyens, B., Brown, P.L., Davis, J.A., Ekberg, C., Kulik, D.A., Missana, T., Tachi, Y., Van Loon, L.R., Altmann, S., 2013. Guidelines for thermodynamic sorption modelling in the context of radioactive waste disposal. Environ. Model. Software 42, 143–156.

Sari, A., Tuzen, M., Citak, D., Soylak, M., 2007. Equilibrium, kinetic and thermodynamic studies of adsorption of Pb(II) from aqueous solution onto Turkish kaolinite clay. J. Hazard Mater. 149, 283–291.

Schnurr, A., Marsac, R., Rabung, T., Lutzenkirchen, J., Geckeis, H., 2015. Sorption of Cm (III) and Eu(III) onto clay minerals under saline conditions: batch adsorption, laser-fluorescence spectroscopy and modeling. Geochem. Cosmochim. Acta 151, 192–202.

Scrudato, R.J., Estes, E.L., 1975. Clay-lead sorption relations. Environ. Geol. 1, 167–170.

Sheikhhosseini, A., Shirvani, M., Shariatmadari, H., 2013. Competitive sorption of nickel, cadmium, zinc and copper on palygorskite and sepiolite silicate clay minerals. Geoderma 192, 249–253.

Soltermann, D., Baeyens, B., Bradbury, M.H., Fernandes, M.M., 2014a. Fe(II) uptake on natural montmorillonites. II. Surface complexation modeling. Environ. Sci. Technol. 48, 8698–8705.

Soltermann, D., Marques Fernandes, M., Baeyens, B., Miehé-Brendlé, J., Dähn, R., 2014b. Competitive Fe(II)–Zn(II) uptake on a synthetic montmorillonite. Environ. Sci. Technol. 48, 190–198.

Sposito, G., 1984. The Surface Chemistry of Soils, New York.

Strawn, D.G., Sparks, D.L., 1999. The use of XAFS to distinguish between inner- and outer-sphere lead adsorption complexes on montmorillonite. J. Colloid Interface Sci. 216, 257–269.

Tournassat, C., Grangeon, S., Leroy, P., Giffaut, E., 2013. Modeling specific pH dependent sorption of divalent metals on montmorillonite surfaces. A review of pitfalls, recent achievements and current challenges. Am. J. Sci. 313, 395–451.

Tournassat, C., Tinnacher, R.M., Grangeon, S., Davis, J.A., 2018. Modeling uranium(VI) adsorption onto montmorillonite under varying carbonate concentrations: a surface complexation model accounting for the spillover effect on surface potential. Geochem. Cosmochim. Acta 220, 291–308.

Uddin, M.K., 2017. A review on the adsorption of heavy metals by clay minerals, with special focus on the past decade. Chem. Eng. J. 308, 438–462.

Ulrich, H.J., Degueldre, C., 1993. The sorption of 210Pb, 210Bi and 210Po on montmorillonite: a study with emphasis on reversibility aspects and on the effect of the

radioactive decay of adsorbed nuclides. ract 62, 81.
Van Bladel, R., Menzel, R., 1969. A thermodynamic study of sodium-strontium exchange on Wyoming bentonite. Proc. Int. Clay Conf. Tokyo 1, 619–634.
Wagner, J.F., 2013. Chapter 5.3 - clay liners and waste disposal. In: Bergaya, F., Lagaly, G. (Eds.), Developments in Clay Science. Elsevier, pp. 663–676.
Westall, J., Zachary, J.L., Morel, F., 1976. MINEQL, a Computer Program for the Calculation of Chemical Equilibrium Composition of Aquous Systems. Technical Note, vol. 18 Department of Civil Engeneer, Massachusetts Institute of Technology, Cambridge, Massachusetts.
Xu, D., Tan, X.L., Chen, C.L., Wang, X.K., 2008. Adsorption of Pb(II) from aqueous solution to MX-80 bentonite: effect of pH, ionic strength, foreign ions and temperature. Appl. Clay Sci. 41, 37–46.
Xu, Y., Liang, X., Xu, Y., Qin, X., Huang, Q., Wang, L., Sun, Y., 2017. Remediation of heavy metal-polluted agricultural soils using clay minerals: a review. Pedosphere 27, 193–204.
Yang, S., Ren, X., Zhao, G., Shi, W., Montavon, G., Grambow, B., Wang, X., 2015. Competitive sorption and selective sequence of Cu(II) and Ni(II) on montmorillonite: Batch, modeling, EPR and XAS studies. Geochem. Cosmochim. Acta 166, 129–145.
Yang, S., Zhao, D., Zhang, H., Lu, S., Chen, L., Yu, X., 2010. Impact of environmental conditions on the sorption behavior of Pb(II) in Na-bentonite suspensions. J. Hazard Mater. 183, 632–640.
Yuan, G.D., Theng, B.K.G., Churchman, G.J., Gates, W.P., 2013. Chapter 5.1 - clays and clay minerals for pollution control. In: Bergaya, F., Lagaly, G. (Eds.), Developments in Clay Science. Elsevier, pp. 587–644.
Zhang, S.Q., Hou, W.G., 2008. Adsorption behavior of Pb(II) on montmorillonite. Colloid. Surface. Physicochem. Eng. Aspect. 320, 92–97.
Zhu, J., Cozzolino, V., Pigna, M., Huang, Q., Caporale, A.G., Violante, A., 2011. Sorption of Cu, Pb and Cr on Na-montmorillonite: competition and effect of major elements. Chemosphere 84, 484–489.
Zhu, R., Chen, Q., Zhou, Q., Xi, Y., Zhu, J., He, H., 2016. Adsorbents based on montmorillonite for contaminant removal from water: a review. Appl. Clay Sci. 123, 239–258.